AIAA JOURNAL
Vol. 40, No. 3, March 2002

# Technical Notes

*TECHNICAL NOTES are short manuscripts describing new developments or important results of a preliminary nature. These Notes cannot exceed six manuscript pages and three figures; a page of text may be substituted for a figure and vice versa. After informal review by the editors, they may be published within a few months of the date of receipt. Style requirements are the same as for regular contributions (see inside back cover).*

## Rise of Total Pressure Near the Stagnation Point on a Sphere

James C. Williams III*
*Auburn University, Auburn, Alabama 36830*

### Introduction

SOME years ago Issa[1] pointed out that, contrary to a common assumption, the total pressure can show an increase in frictional flow. He showed that viscous stresses could result in a rise in total pressure for 1) the plane stagnation point flow and 2) the Stokes flow past a sphere, for which exact solutions exist. Later, van Ondheusden[2] pointed out that this is a problem of practical physical significance because it relates to the viscous effect on pitot tube readings at low Reynolds number. He further specialized the solutions of Heinmenz and Homann (see Schlichting[3]) for plane and axisymmetric stagnation point flows, respectively, to the case of the stagnation point on a cylinder and sphere, arriving at expressions for the stagnation point pressure coefficient, $C_{p0} = [2(p_0 - p_\infty)/\rho U_\infty^2]$, of $C_{p0} = 1 + 4/Re$ for a cylinder and $C_{p0} = 1 + 6/Re$ for a sphere. Here $Re = U_\infty a/\nu$ is the Reynolds number based on the body radius. He also noted that, for a sphere at low Reynolds number, Stokes flow predicts $C_{p0} = 3/Re$. The Stokes flow solution is only valid for low Reynolds numbers as a result of the basic assumptions inherent in the theory. It is important to recall also that the solutions for the two-dimensional stagnation point (Heinmenz) and for the axisymmetric stagnation point (Homann) are only valid for large Reynolds numbers, where the flowfield may be divided into two parts, a viscous inner flow and an inviscid (irrotational) outer flow.

The purpose of the present work is to show that for the flow past a sphere or a spherically tipped body, the latter assumption, that the viscous layer must match a known inviscid outer flow, is not necessary; it is possible to obtain exact solutions to the Navier–Stokes equations for flow in the vicinity of the forward stagnation streamline. These solutions extend a large distance from the body and satisfy the uniform flow condition at infinity instead of some inviscid flow boundary conditions. Solutions may be found, therefore, for any Reynolds number, no matter how large or small. At high Reynolds numbers, the present solutions include both the outer, predominately inviscid flow and the inner, predominately viscous flow and reduce to the classical solution of Homann.[4] For low Reynolds numbers, the present results match those of Stokes flow. The resulting exact solutions are used here to predict the rise in the stagnation pressure (coefficient) over the entire range of Reynolds numbers.

### Analysis

We consider the flow in the vicinity of the forward stagnation streamline on a sphere or spherically tipped body. It is assumed that the flow is steady and incompressible and that the fluid has constant properties. Because the body is assumed to be a sphere (or to be spherically tipped), the appropriate coordinate system in which to describe the body in the region of the spherical tip and to analyze the flow is a spherical coordinate system, with the origin of coordinate system located at the center of the sphere, as shown in Fig. 1. The flow far ahead of the body is uniform with a velocity $U_\infty$ directed along the negative $z$ axis.

In the present problem, it is more convenient to work with the stream function and vorticity in spherical coordinates rather than the velocity components and pressure directly. The flow under consideration is axisymmetric so that the velocity in the $\varphi$ direction, $v_\varphi$, and the gradient in the $\varphi$ direction both vanish ($\partial/\partial\varphi = v_\varphi = 0$). As a result of this symmetry, the $r$ and $\theta$ components of the vorticity vector, $\zeta_r$ and $\zeta_\theta$, vanish. We introduce a stream function $\psi$ in nondimensional form, $\psi^* = \psi/U_\infty a^2$, defined such that the continuity equation is satisfied identically, that is,

$$r^{*2} v_r^* \sin\theta = -\frac{\partial \psi^*}{\partial \theta}, \qquad r^* v_\theta^* \sin\theta = \frac{\partial \psi^*}{\partial r^*}$$

Here $a$ is the radius of the sphere and the nondimensional radial coordinate and velocities are given by $r^* = r/a$, $v_r^* = v_r/U_\infty$, and $v_\theta^* = v_\theta/U_\infty$. The nondimensional $\varphi$ component of vorticity, $\zeta^* = \zeta_\varphi a/U_\infty$, is given in terms of the stream function by

$$\zeta^* = \frac{1}{r^* \sin\theta}\frac{\partial^2 \psi^*}{\partial r^{*2}} - \frac{\cot\theta}{r^{*3}\sin\theta}\frac{\partial \psi^*}{\partial \theta} + \frac{1}{r^{*3}\sin\theta}\frac{\partial^2 \psi^*}{\partial \theta^2} \qquad (1)$$

The vorticity transport equation, which is obtained by eliminating the pressure from the $r$ and $\theta$ momentum equations by cross differentiation, is in nondimensional form

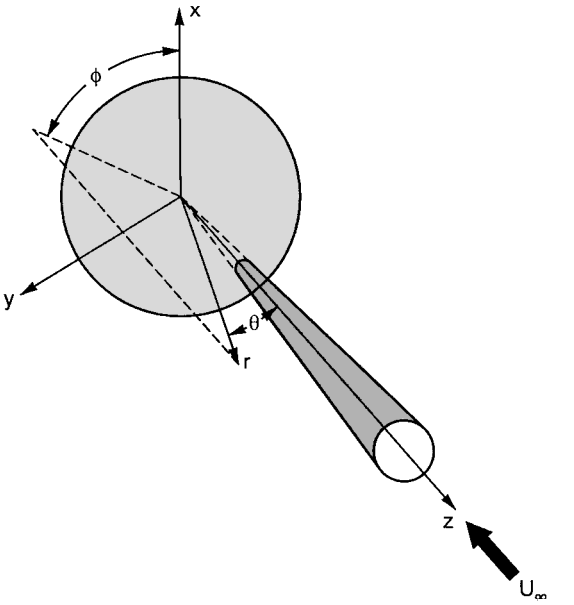


**Fig. 1 Spherical coordinate system showing sphere, freestream velocity, and region of analysis validity.**

Received 12 December 2000; revision received 26 October 2001; accepted for publication 27 November 2001. Copyright © 2001 by the American Institute of Aeronautics and Astronautics, Inc. All rights reserved. Copies of this paper may be made for personal or internal use, on condition that the copier pay the $10.00 per-copy fee to the Copyright Clearance Center, Inc., 222 Rosewood Drive, Danvers, MA 01923; include the code 0001-1452/02 $10.00 in correspondence with the CCC.

*Professor Emeritus, Department of Aerospace Engineering. Associate Fellow AIAA.

$$Re\left\{-\frac{1}{r^{*2}\sin\theta}\frac{\partial\psi^*}{\partial\theta}\frac{\partial\zeta^*}{\partial r^*}+\frac{1}{r^{*2}\sin\theta}\frac{\partial\psi^*}{\partial r^*}\frac{\partial\zeta^*}{\partial\theta}+\frac{\zeta^*}{r^*}\left[-\frac{1}{\sin\theta}\frac{\partial}{\partial r^*}\left(\frac{1}{r^*}\frac{\partial\psi^*}{\partial\theta}\right)+\frac{1}{r^*}\frac{\partial}{\partial\theta}\left(\frac{1}{\sin\theta}\frac{\partial\psi^*}{\partial r^*}\right)\right]\right\}$$
$$=\frac{1}{r^{*2}}\frac{\partial}{\partial r^*}\left(r^{*2}\frac{\partial\zeta^*}{\partial r^*}\right)+\frac{1}{r^{*2}\sin\theta}\frac{\partial}{\partial\theta}\left(\sin\theta\frac{\partial\zeta^*}{\partial\theta}\right)-\frac{\zeta^*}{r^{*2}\sin^2\theta} \tag{2}$$

where the Reynolds number is $Re=\rho U_\infty a/\mu$. At this point, Eqs. (1) and (2) are completely general. They are the definition of vorticity and the vorticity transport equation, respectively, written in a spherical coordinate system for the axisymmetric flow defined earlier.

The boundary conditions on the body surface are then $v_r^*(1,\theta)=v_\theta^*(1,\theta)=0$. In terms of the stream function these become

$$\frac{\partial\psi^*}{\partial\theta}=0,\qquad \frac{\partial\psi^*}{\partial r^*}=0$$

Far from the body, the velocity must be uniform along the negative $z$ axis so that we have

$$\lim_{r^*\to\infty}\frac{1}{r^{*2}\sin\theta}\frac{\partial\psi^*}{\partial\theta}=\cos\theta,\qquad \lim_{r^*\to\infty}\frac{1}{r^*\sin\theta}\frac{\partial\psi^*}{\partial r^*}=\sin\theta$$

The only boundary condition available for the vorticity arises from the fact that the vorticity must vanish far from the body, that is,

$$\lim_{r^*\to\infty}\zeta_\varphi^*=0$$

In view of the fact that we expect the flowfield to extend far from the body, at least at the lower Reynolds numbers, it is convenient to introduce the new coordinate $\xi(r^*)$ defined by $r^*=e^\xi$. The nondimensional stream function for the freestream flow is $\psi^*=e^{2\xi}\sin^2\theta/2$. Guided by this stream function, we take in the present case a nondimensional stream function and vorticity of

$$\psi^*=(e^{2\xi}/2)f(\xi)\sin^2\theta,\qquad \zeta^*=g(\xi)\sin\theta$$

Introducing these into the vorticity transport equation and the equation defining vorticity, we obtain

$$g''+g'-2g=e^\xi Re\cos\theta\{-fg'+gf\} \tag{3a}$$

$$f''+3f'=2ge^\xi \tag{3b}$$

where primes denote differentiation with respect to $\xi$. We now make the assumption that $\theta$ is small so that $\cos\theta\approx 1$, and Eqs. (3a) and (3b) become

$$g''+g'-2g=e^\xi Re\{-fg'+gf\} \tag{4a}$$

$$f''+3f'=2ge^\xi \tag{4b}$$

Equations (4a) and (4b) are the equations to be solved to yield the stream function and vorticity field and, hence, the velocity field. The only assumption we have made is that the angle $\theta$ is small so that $\cos\theta\approx 1$. This means that the solution is limited to that portion of the conical region, whose axis coincides with the $z$ axis, whose apex is at the origin of the coordinate system and which lies outside the sphere (Fig. 1), that is, to the vicinity of the forward stagnation streamline.

The velocity components are given by

$$v_r^*=-f(\xi)\cos\theta\approx -f(\xi)$$

$$v_\theta^*=\sin\theta\{f(\xi)+[f'(\xi)/2]\}\approx\theta\{f(\xi)+[f'(\xi)/2]\}$$

In each case, the last expression results from the approximation $\theta\ll 1$. Now if $x$ is the distance along the body surface measured from the stagnation point so that $x=a\theta$, the normalized velocity component along the surface $v_\theta^*$ is, with the small angle approximation, $v_\theta^*=(x/a)(f+f'/2)$ It is clear that the small-angle approximation is equivalent to the approximation $u\approx x$ made in the classical stagnation point solutions. In the present case, however, we do not propose to match an external inviscid flow solution, as in the classical case, but to satisfy the boundary conditions far from the body, that is, $v_\theta^*=\sin\theta$ and $v_r^*=-\cos\theta$.

On the surface of the body, both velocity components must vanish so that we have as boundary conditions on the body $f(0)=f'(0)=0$. Far from the body, the flow must match the external uniform flow so that we have

$$\lim_{\xi\to\infty}f(\xi)=1$$

so that we match the inviscid flow $\psi^*=r^{*2}\sin\theta/2$. In addition, because the flow far from the body is irrotational, we have the boundary condition on $g$ of

$$\lim_{\xi\to\infty}g(\xi)=0$$

We note that we have two second-order equations in $g(\xi)$ and $f(\xi)$ [Eqs. (4a) and (4b)] but that we have three boundary conditions on $f(\xi)$ and only one on $g(\xi)$. This situation will pose some difficulties, to be discussed later, but these difficulties are not insurmountable.

Equations (4a) and (4b) may now be solved as a set of coupled nonlinear ordinary differential equations with a set of three boundary conditions on $f(\xi)$ (two-boundary conditions at the wall and one applicable as $\xi\to\infty$) and a single boundary condition for $g(\xi)$. As already mentioned, this odd arrangement for boundary conditions causes some problems. In principle, this problem could be solved by a shooting technique in which one assumes values of $f''(\xi=0)$ and $g(\xi=0)$, marches in the direction of increasing $\xi$, and determines if the outer boundary conditions are satisfied. One would iterate on the initial guesses until the outer boundary conditions are satisfied. This technique is cumbersome to say the least. A better technique has been devised and involves an additional transformation: $g^*(\xi)=g(\xi)/g(0)=g(\xi)/g_0$ and $h(\xi)=f(\xi)/g_0$. In terms of these new variables, Eqs. (4a) and (4b) become

$$g^{*\prime\prime}+g^{*\prime}-2g^*=e^\xi Re\,g_0(-hg^{*\prime}+hg^*) \tag{5a}$$

$$h''+3h'=2g^*e^\xi \tag{5b}$$

with boundary conditions $h(0)=h'(0)=0$, $g^*(0)=1$, and

$$\lim_{\xi\to 0}g^*=0$$

The remaining boundary condition is used to determine $g_0$ from

$$\lim_{\xi\to\infty}h(\xi)=\frac{1}{g_0}\lim_{\xi\to\infty}f(\xi)=\frac{1}{g_0}$$

With this formulation, there is a straightforward iteration procedure for solving Eqs. (5a) and (5b). An initial assumption is made for function $g^*(\xi)$, and this function is employed in Eq. (5b). This is then integrated as an initial value problem using a fourth order Runge–Kutta numerical integration method. This integration is carried out to a large value of $\xi$, for example, $\xi_{\max}$, where $\mathrm{d}h/\mathrm{d}\xi=0$ (typically $\xi_{\max}\approx 10$); at this point $g_0$ is obtained from $g_0=1/h(\xi_{\max})$. When this provisional value of $g_0$ and the provisional distribution of $h(\xi)$ are used, the nonlinear coefficients in Eq. (5a) are evaluated, and Eq. (5a) is cast in the form

$$g^{*\prime\prime}+\alpha_1 g^{*\prime}+\alpha_2 g^*=0 \tag{6}$$

with the coefficients $\alpha_1(\xi)$ and $\alpha_2(\xi)$ known. Equation (6) is solved using the Thomas algorithm to yield an updated $g^*$. This new $g^*$ is employed in Eq. (5a) to obtain a new $h(\xi)$ and $g_0$, which in turn are used to obtain a new $g^*(\xi)$ from Eq. (6). This procedure is repeated iteratively until two successive solutions of Eq. (6) are the same to within a small tolerance. The final distribution $g^*$ is then employed once more in Eq. (5b) to obtain a final $h(\xi)$, $g_0$, and $f(\xi)$. When this procedure is used, convergence is relatively rapid, occurring generally in 6–14 iterations.

## Results

Numerical solutions have been obtained for Eqs. (5a) and (5b) with appropriate boundary conditions, for a number of Reynolds

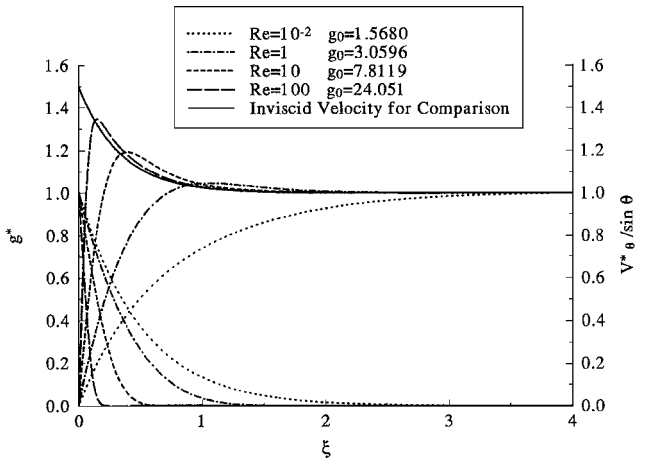


**Fig. 2 Velocity and vorticity profiles near the stagnation point. (The upper set of curves shows the velocity, and the lower set shows the vorticity.)**

numbers ranging from $10^{-2}$ to $10^{6}$. The numerical results provide the normalized stream function, which can be used to determine the velocity distribution, the wall vorticity, and the normalized vorticity distribution. Typical velocity distributions, $v_\theta^*/\sin\theta(\xi)$, and vorticity distributions, $g^*(\xi)$, as well as the appropriate values of $g^*(0)$ are presented in Fig. 2 for Reynolds numbers of $10^{-2}$, 1, 10, and 100. For comparison, Fig. 2 also contains the inviscid velocity distribution $v_\theta^*/\sin\theta(\xi)$.

In general, the normalized vorticity $g^*(\xi)$ varies from unity at the wall ($\xi = 0$) to zero far from the body (left-hand scale), whereas the velocity $v_\theta^*/\sin\theta(\xi)$ varies from zero at the wall ($\xi = 0$) to unity far from the body (right-hand scale).

For a Reynolds number of $10^{-2}$, the effects of viscosity extend to approximately $\xi = 3.5$ or 32.12 radii from the body. The vorticity layer is very thick, and the only really inviscid part of the flow is found far from the body in the freestream. These results are in fact very close to the Stokes flow limit. As the Reynolds number is increased, the extent of the viscous layer is reduced, and there is clearly a displacement effect in which the velocity $v_\theta^*/\sin\theta$ lies above the potential flow velocity. At a Reynolds number of 1, the viscous layer is still quite thick, extending to approximately $\xi = 1.75$ (or to a radius of 5.75 times the sphere radius). The peak velocity, however, is nowhere near that for potential flow velocity at the sphere (1.5). Beyond $\xi = 1.75$, the flow is essentially inviscid, but the freestream flow is not reached until somewhere about $\xi = 2.5$ or $r = 12.18a$. Similar results are shown for a Reynolds number of 10.

As the Reynolds number is increased, the viscous region of the flow becomes smaller until at Reynolds numbers greater than $10^4$ the flow has essentially reached conditions where boundary-layer theory is valid. The viscous layer is quite thin, extending only to $\xi = 0.02$ ($r = 1.02a$) at $Re = 10^4$, only to $\xi = 0.0068$ ($r = 1.0068a$) at $Re = 10^5$, and only to $\xi = 0.0023$ ($r = 1.0023a$) at $Re = 10^6$. There is very little or no displacement effect. (The actual velocity profile lies on the potential flow velocity, once they meet.) The peak velocity in the viscous flow is 1.4758 at $Re = 10^4$, 1.4913 at $Re = 10^5$, and 1.4970 at $Re = 10^6$.

As a practical matter, we are interested in the stagnation point pressure coefficient $C_{p0} = 2[p(a,0) - p_\infty]/\rho U_\infty^2$. This can be obtained once the solutions outlined earlier are determined. Turning to the $r$ and $\theta$ momentum equations and introducing the stream function, we obtain

$$\frac{\partial p^*}{\partial \xi} = -ff' - \frac{\cos\theta}{Re}e^{-\xi}\,(f'' + 3f') + \sin^2\theta\left(\frac{3}{2}ff' + \frac{1}{4}f'^2\right)$$

$$\frac{\partial p^*}{\partial \theta} = \frac{\sin\theta e^{-\xi}}{Re}\left(\frac{1}{2}f''' + \frac{3}{2}f'' - \frac{1}{2}f' - f\right) + \sin\theta\cos\theta\left(ff' - \frac{f'^2}{4}\right)$$

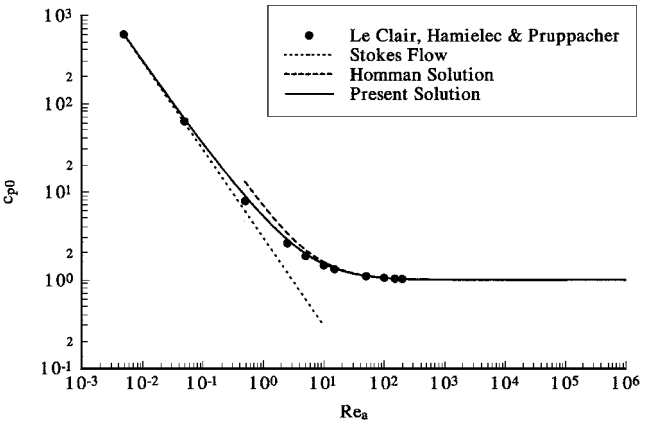


**Fig. 3 Variation of the stagnation point pressure coefficient with Reynolds number.**

Integrating these, limiting ourselves to the forward stagnation point ($\theta = 0$), and introducing the definition of vorticity, we obtain

$$C_{p0} = 1 + \frac{4g_0}{Re}\int_0^\infty g^*\,\mathrm{d}\xi$$

When the wall vorticity $g^*(0)$ and the vorticity distributions $g^*(\xi)$ obtained from the earlier solutions are used, the stagnation point pressure coefficient $C_{p0}$ has been computed for a range of Reynolds numbers from $10^{-2}$ to $10^6$. The results of these computations are presented in Fig. 3.

Also shown on Fig. 3 are the Stokes flow solution and the solution for the stagnation flow in the vicinity of an axisymmetric stagnation point[4] as adapted to the sphere by van Ondheusden.[2] Clearly the present solution bridges the gap between the Stokes flow solution, which appears to be valid for Reynolds number $Re_a$ less than approximately $2 \times 10^{-2}$, and the Homan solution, which appears to be valid for $Re_a > 20$. As a check, the results of the exact solutions to the Navier–Stokes equations for flow past a sphere that have been obtained for certain discrete Reynolds numbers by LeClair et al.[5] are indicated in Fig. 3. The present exact solutions to the Navier–Stokes equations for flow in the vicinity of the forward stagnation streamline provide an very good prediction of the stagnation point pressure coefficient over the entire Reynolds number range.

The present results were obtained using the technique described, using successively smaller step sizes, and then extrapolating to zero step size. The numerical accuracy of the solutions reported here may be assessed by comparing the results of these solutions with exact solutions that exist at the low and high Reynolds number extremes. A numerical solution was obtained for a Reynolds number of zero where an exact solution, the Stokes solution, is known. The Stokes flow solution yields for the wall vorticity $g^*(0)/\sin\theta$ the value $\frac{3}{2}$ and for the quantity

$$4g(0)\int_0^\infty g^*(\xi)\,\mathrm{d}\xi$$

(which is used in evaluating the stagnation point pressure coefficient) the value 3.0. The numerical solution for zero Reynolds number yields, for these two quantities, the values 1.500248 and 3.000301, respectively, for corresponding numerical errors of 0.0166 and 0.0100%, respectively. In addition, the solution obtained here was compared to the classical solution, presented in Ref. 3, and the solutions for the normalized vorticity and normalized stream function were in agreement with the exact solution to at least six decimal places.

At high Reynolds numbers, Homann's solution, as adopted for a sphere by Ondheusden,[2] is used. This solution yields, at a Reynolds number of $10^6$, values of $g_0^*$ and

$$4g(0)\int_0^\infty g^*(\xi)\,\mathrm{d}\xi$$

of 2410.2979 and 6.00. The present numerical solution for a Reynolds number of $10^6$ yields corresponding values of 2412.6741

and 5.9972 for computational errors of 0.0944 and 0.0464%, respectively. Clearly the numerical solutions offer a high degree of accuracy.

## Conclusions

A new exact solution to the Navier–Stokes equations for flow in the vicinity of the forward stagnation streamline on a sphere has been developed. These solutions describe the flowfield all of the way from the body surface to the uniform flow far from the body, in contrast to the traditional stagnation point solutions and, hence, may be used to obtain solutions for the entire range of Reynolds numbers. Solutions have been obtained for the vorticity field and the stream function field for Reynolds numbers from $10^{-2}$ to $10^{6}$, and these solutions have been used to calculate the stagnation point pressure coefficient on a sphere for this Reynolds number range. The results provide an excellent prediction of the stagnation point pressure coefficient over the entire Reynolds number range.

## References

[1]Issa, R. I., "Rise of Total Pressure in Frictional Flow," *AIAA Journal*, Vol. 33, No. 4, 1995, pp. 772–774.

[2]Van Ondhensden, B. W., "Comment on 'Rise of Total Pressure in Frictional Flow,'" *AIAA Journal*, Vol. 35, No. 2, 1996, pp. 426–427.

[3]Schlichting, H., *Boundary Layer Theory*, McGraw–Hill, New York, 1979, pp. 95–101.

[4]Homann, F., "Der Einfluss grosser Zähigkeit bei der Strömmung um den Zylinder und um die Kugel," *Zeitschrift für Angewandte Mathemik und Mechanik*, Vol. 16, No. 3, 1936, p. 153.

[5]LeClair, B. P., Hamielec, A. E., and Pruppacher, H. R., "A Numerical Study of the Drag on a Sphere at Low and Intermediate Reynolds Numbers," *Journal of the Atmospheric Sciences*, Vol. 27, No. 2, 1970, pp. 308–315.

J. C. Hermanson
*Associate Editor*

# Symmetry Properties of the Transitional Sphere Wake

R. Mittal* and J. J. Wilson†
*University of Florida, Gainesville, Florida 32611*
and
F. M. Najjar‡
*University of Illinois at Urbana–Champaign, Urbana, Illinois 61801*

## Introduction

On the basis of previous studies,[1–11] it is reasonable to state that the various bifurcations as well as the vortex dynamics in the wake of a sphere are relatively well understood up to a Reynolds number (based on sphere diameter $D$ and freestream velocity $U_\infty$) of about 350. In particular, it is known that the axisymmetric, steady wake first becomes unstable to nonaxisymmetric perturbations at a Reynolds number of about 210 (Ref. 7). The next bifurcation occurs at a Reynolds number of about 277 and leads to the establishment of time-periodic shedding[10] of vortex loops. In this shedding mode vortex loops are formed precisely at the same azimuthal location in every cycle, and the wake maintains strict symmetry at every time instant about a fixed plane that passes through the wake centerline.[5] The orientation of the symmetry plane is determined in simulations by the initial conditions. Studies[5,8] also indicate that strict planar symmetry is lost somewhere between 350 and 375, but to date there is no clear consensus on the nature of the vortex formation process at these higher Reynolds numbers. Most studies[9,10] implicitly assume that the vortex loops do not have any preferred orientation and that the time-averaged wake is axisymmetric about the wake centerline.

The objective of this Note is to use direct numerical simulation (DNS) data of flow past a sphere to analyze the symmetry properties of the time-averaged wake in the range $500 \le Re \le 1000$. To this end, an accurate Fourier–Chebyshev spectral collocation method has been used for computing three-dimensional, unsteady, viscous incompressible flow past a sphere where time advancement is through a second-order-accurate time-split scheme. The current solver has been validated extensively[4] in the Reynolds number range $50 < Re < 500$ against established experimental data. A detailed description of the solver and validation study, as well as other computed results can be found in Refs. 4, 5, and 12.

Results of DNS at three Reynolds numbers (500, 650, and 1000) are reported here. The outer domain size for these simulations is $25D$, and the grid for each simulation is chosen so as to ensure at least five orders of magnitude decay in the wave-number spectra of the flow variables. This results in a grid with $6.4 \times 10^5$ ($1.3 \times 10^6$) collocation points for the $Re = 500$ ($Re = 1000$) simulation. Initially, a mean axisymmetric flow is obtained. Subsequently, a small perturbation in the form of a random (white noise) azimuthal slip velocity is provided on the sphere surface for a short time. This perturbation is random in space and therefore does not have a preferred spatial structure or orientation. The disturbance grows in time as a result of the inherent instability of the flow and eventually saturates, at which point data are extracted for analysis.

## Discussion of Results

The force on the sphere is decomposed into three components: the drag force $F_d$, which acts in the streamwise ($x$-) direction, and the two components of the side force ($F_y$ and $F_z$), which act perpendicular to the drag force. The magnitude of the side force can be computed as $F_s = \sqrt{(F_y^2 + F_z^2)}$. Figure 1 shows the variation of the drag $C_d$ and side force $C_s$ coefficients with time. The mean values of the drag coefficient for $Re = 500$, 650, and 1000 are computed to be 0.56, 0.52, and 0.47, respectively, and these are in very good agreement with experiments.[13] The side-force coefficients show a complex behavior with magnitudes that are roughly an order smaller than those of the drag coefficient.

Based on all of the data that have been analyzed,[14] the dominant nondimensional shedding frequency ($fD/U_\infty$, where $f$ is the shedding frequency) lies in the range from 0.17 to 0.19 for the entire range of Reynolds numbers simulated here, and this is in line with experiments.[10] In addition, the current simulations indicate the presence of a low frequency in the near wake with nondimensional frequency equal to 0.05 for all of the three Reynolds numbers investigated. Despite similar previous observations,[8,9,11] the dynamics associated with this low frequency are not currently well understood.

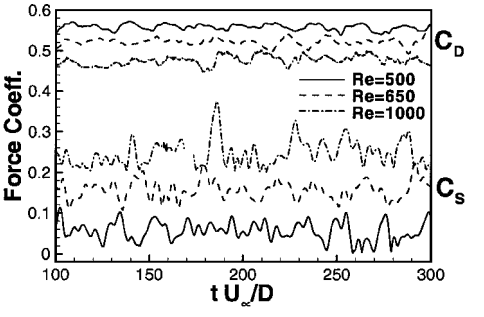


**Fig. 1 Temporal variation of drag and side-force coefficients. The side-force coefficients for $Re = 650$ and 1000 have been offset in the vertical direction by +0.1 and +0.2 respectively.**

Received 5 May 2001; revision received 6 November 2001; accepted for publication 12 November 2001. Copyright © 2001 by the American Institute of Aeronautics and Astronautics, Inc. All rights reserved. Copies of this paper may be made for personal or internal use, on condition that the copier pay the $10.00 per-copy fee to the Copyright Clearance Center, Inc., 222 Rosewood Drive, Danvers, MA 01923; include the code 0001-1452/02 $10.00 in correspondence with the CCC.

*Assistant Professor, Department of Mechanical Engineering; currently Assistant Professor, Department of Mechanical and Aerospace Engineering, George Washington University, Washington, DC 20052. Member AIAA.

†Graduate Student, Department of Mechanical Engineering.

‡Principal Research Scientist, Center for Simulation of Advanced Rockets. Member AIAA.